Wide-spectrum cancer killing by ENDOD1 ablation

Zizhi Tang[1], Ming Zeng[1], Xiaojun Wang[1], Antony M. Carr[2,*], Cong Liu[1,*]

[1]Department of Paediatrics, Key Laboratory of Birth Defects and Related Diseases of Women and Children (Ministry of Education), West China Second University Hospital, Sichuan University, Chengdu, 610041, China.

[2]Genome Damage and Stability Centre, School of Life Science, University of Sussex, Falmer, BN1 9RQ, UK.

Corresponding authors: C.L.: congliu@scu.edu.cn

A.M.C.: a.m.carr@sussex.ac.uk

Summary

Conventional cytotoxic cancer therapy is limited by adverse side-effects on non-affected tissues. Conversely, synthetic lethal anti-cancer approaches have the potential to reduce systemic cytotoxicity, but most potential synthetic lethality targets are not wide-spectrum and thus the subtype-specific drug targets each have limited application. We identified endonuclease D1 (ENDOD1) in a proteomic characterization of the biological response of PARP inhibition and show that ENDOD1 is recruited to PAR-positive single strand breaks, where it influences the kinetics of single-strand break repair. As with PARPi, ENDOD1 depletion triggered DNA double strand breaks in cycling cells when homologous recombination repair was defective. However, unlike PARPi, ENDOD1 depletion prompted the generation of tracts of single strand DNA in both cycling and G1 arrested p53 defective cells. This identifies a new synthetic lethal interaction that we show encompasses the majority of *TP53* hotspot mutations. We conclude that *ENDOD1* is a promising wide-spectrum anti-cancer drug target.

Recent success in targeting homologous recombination defective (HRD) cancers by PARP inhibitor (PARPi) treatment paved a new route for cancer subtype-specific chemotherapy [1]. PARPi's (i.e. Olaparib [2] and Talazoparib [3]) enzymatically inactivate and trap PARPs to DNA breaks, necessitating functional homologous recombination (HR) to avoid cytotoxicity [4]. During a characterization of PARPi-induced DNA damage responses in the presence and absence of the Hepatitis B virus protein HBx [5], which induces a HRD by depleting $CUL4^{WDR70}$, we detected an increase in endonuclease domain-containing protein 1 (ENDOD1) peptides following six days of Olaparib treatment (data not shown and Supplementary Figure 1).

Previous studies have demonstrated that ENDOD1 is a cytoplasmic nuclease (Figure 1a) involved in innate immunity as part of the RNF26-mediated cGAS-STING pathway [6]. The unexpected identification of ENDOD1 as a PARPi-responsive protein lead us to examine its potential role in DNA repair. *ENDOD1* knockout RPE1 cells showed moderate sensitivities to CPT, cisplatin and the G4 inhibitor Cx5461. No detectable sensitivity was observed upon IR or HU treatment (Supplementary Figure 2a). Unexpectedly, *ENDOD1*$^{-/-}$ RPE1 cells displayed obvious resistance to the single strand break (SSB)-inducing agent hydrogen peroxide (H_2O_2) (Supplementary Figure 2b). A similar resistance to H_2O_2 was observed for GES-1, a normal gastric epithelial line, following siRNA against ENDOD1 (Supplementary Figure 2b).

Indirect immunofluorescent staining of untreated RPE1 cells revealed predominant cytoplasmic localization of ENDOD1 (Figure 1b, top panel). 10 minutes following H_2O_2 challenge ENDOD1 was also visible in the nucleus, where it colocalized with PAR-positive foci (Figure 1b, bottom two panels). Using single cell electrophoresis under denaturing conditions (alkaline comet assay) to assess repair kinetics of gap and nicks, we did not detect a major repair defect between proliferating *ENDOD1*$^{-/-}$ and RPE1 control cells (Figure 1c, left two panels). When cells were arrested in G1 phase upon serum starvation before treatment, despite the clearance of SSBs in *ENDOD*1$^{-/-}$ being higher in the early phase of repair, the overall repair over time was slower when compared with RPE1 (Figure 1c, right panel). Moreover, gene silencing of SSB repair proteins re-sensitized G1 arrested *ENDOD1*$^{-/-}$ cells to H_2O_2 as depletion of *XRCC1*, *Ligase 3* and *TDP1* exacerbated cell killing (Figure 2a). This suggests that the enhanced survival involves the classical SSB repair machinery [7] Taken together, these data are consistent with ENDOD1 influencing SSB repair.

Previous studies showed homologous recombination (HR) factors, including BRCA1, BRCA2 and Fanconi Anaemia proteins, are required for DNA repair following PARP inhibition and that compromising the HR pathway results in synthetic lethality with PARPi [8]. To examine if ENDOD1 participates in PARP regulation, we carried out survival assays in cells compromised for ENDOD1 function combined with ablation of selected HR genes. Mirroring PARP inhibition, ablating *ENDOD1* by siRNA killed cells that were co-depleted for *BRCA1*, *BRCA2*, *CTIP*, *EXO1*, *FACND2* and *WDR70* (Figure 2b and Supplementary Figure 3a). In contrast, HR-competent untransformed cells (including RPE1 and GES-1) exhibited no proliferation defects upon ablation of *ENDOD1*, other than a minor accumulation of cells in G1 (Supplementary Figure 3b-c). This is consistent with slower SSB repair in G1 (Figure 1c). PARPi-induced HRD cell death coincides with the generation of toxic DNA structures and chromosomal aberration [4]. Consistent with this, *BRCA1* siRNA treatment of *ENDOD1*$^{-/-}$ cells resulted in increased γH2AX and 53BP1 foci, indicative of increased DNA double strand breaks (DSBs) (Figure 2c). Similarly, depleting *BRCA2* in *ENDOD1*$^{-/-}$ cells elevated 53BP1 foci formation (Figure 2d). Thus, we conclude that loss of ENDOD1 function phenocopies PARPi in compromising the genomic integrity of HR-defective cells.

To establish if ENDOD1 loss of function could compromise the viability of HRD tumour cells we depleted *ENDOD1* in a collection of cancer cell lines. To our surprise *ENDOD1* depletion significantly reduced the viability of ~80% of the tested cell lines, irrespective of their reported HR status (Supplementary Figure 4a). By examining the known characteristics of the cell lines we correlated si*ENDOD1*-induced lethality in HR proficient cells with *TP53* mutation spanning the common hotspot areas (R248, R273) found in most malignancies (Figure 3a) [9]. Cell lines such as A549 and MDA-MB-361 that do not carry *TP53* or HR mutations were not sensitive to si*ENDOD1* (Supplementary Figure 4b). We validated the synthetic lethality between p53 and ENDOD1 in our *ENDOD1*$^{-/-}$ and RPE1 control cells. While *ENDOD1*$^{-/-}$ and RPE1 si*TP53* cells were viable, *ENDOD1*$^{-/-}$ si*TP53* cells arrested in G1 within 60 hours (Supplementary Figure 4c) and cell death became apparent at 5 days and was extensive after 7 days (Figure 3b and Supplementary Figure 4d). The killing effect of *ENDOD1*$^{-/-}$ si*TP53* was also apparent in G1-arrested non cycling cells (Figure 3c), suggesting that the cytotoxicity is independent of DNA replication. We conclude that ablation of *ENDOD1* is synthetic lethal to cells with functional loss of *TP53*.

To further characterise the synthetic lethal interaction between ENDOD1 and

p53 we used comet assays to assess DNA lesions occurring in G1 arrested *ENDOD1*$^{-/-}$ and control RPE1 cell following si*TP53*. Alkaline comet assays revealed that si*TP53* induced a high level of DNA breaks in *ENDOD1*$^{-/-}$ but not RPE1 cells (Figure 3d-e). Neutral comet assays did not show an increase in DNA damage in the same experiment. Thus, these breaks were likely in the form of SSBs. Consistent with this, analysis of phosphorylated RPA32 Serine 33 (pRPA32), a typical marker of single stranded DNA (ssDNA), showed that pRPA32 staining was elevated in the nuclei of either proliferating or G1 arrested *ENDOD1*$^{-/-}$ cells treated with si*TP53*, but was not elevated in the RPE1 cells treated with si*TP53* or control *ENDOD1*$^{-/-}$ (Figure 4a-b). In sharp contrast to this indicator of ssDNA lesions, 53BP1 foci, which are surrogates for DSBs, were not significantly increased in G1-arrested *ENDOD1*$^{-/-}$ cells 48-96 hours after si*TP53* transfection (Figure 4c). We conclude that *TP53* and *ENDOD1* function co-ordinately to prevent cell inviability arising from the untimely generation of detrimental ssDNA structures.

TP53 mutations in human cancers exhibits diverse functional consequences including loss- and gain-of-function [10]. A recent study reported PARP-dependent rapid recruitment of p53 to sites of DNA damage. This recruitment required the DNA binding and carboxyl terminal domains of p53 [11]. We therefore assayed the production of pRPA32 foci upon si*ENDOD1* in a range of cell lines with defined *TP53* mutations. si*ENDOD1*-induced pRPA32 foci were detected in G1 phase of cancer lines harbouring *TP53* null (SKOV-3 and NCI-H1299) as well as gain of function (GOF) mutations such as *R273C* (C33A) and *R273H* (MBA-MD-468), but no signal was apparent in *TP53* competent line A549 (Figure 4d).

Our characterisation of *ENDOD1* depletion in cancer-relevant backgrounds has identified synthetic lethality with two specific backgrounds: HRD and mutant *TP53*. We showed that loss of ENDOD1 function generates lethal DNA structures in cells harbouring either HR or p53 defects. Interestingly, these two synthetic lethal interactions can be mechanistically separated: for the synthetic lethality we observed in HRD cells, the cytotoxicity resembles that of PARPi, involving the formation of DSBs. In contrast, for the synthetic lethality observed between ENDOD1 and p53 loss of function, the cytotoxicity is associated with the formation of tracts of ssDNA and this can occur in G1 arrested cells without progress into S phase. This defines a novel DNA damaging activity that is distinct those engendered by PARPi.

In summary, we have characterised the consequences of loss of ENDOD1

function in the context of genotoxic stress and genetic backgrounds commonly found in cancer cells. Our discovery that *ENDOD1* depletion bestows specific synthetic lethality with mutations in the high-incidence tumour suppressor *TP53* suggests a novel route for wide-spectrum cancer treatment.

Methods and Materials

Cell culture

The *ENDOD1*$^{-/-}$ clone was obtained by targeting exon 1 with gRNA (5'-CAGCCTCTTCGCCCTGGCTGG-3') in RPE1 cells. The resulting insertion (C→CG) creates a frameshift in the ORF at amino acid position Arg4. All human cell lines were cultured in complete media supplemented with 10 or 20% foetal bovine serum (FBS) according to ATCC protocols. Where indicated, G1 arrest was induced by serum starvation for 8-11 days in complete media: RPE1 and *ENDOD1*$^{-/-}$, 1% FBS; GES-1, SKOV-3, NCI-H1299, MBA-MD-468 and C33A, 0.5% FBS. All cell lines tested negative for mycoplasma contamination. Double stranded siRNA were obtained from Ribobio, Guangzhou, China. Plasmid and siRNA transfections were performed using Lipofectamine 3000 (Invitrogen). 1 ug plasmid or 50 nM siRNA were applied per 10^6 cells unless otherwise stated.

Chemicals and genotoxic treatments

To induce DNA damage, cells were treated with the indicated concentrations of: CPT (Selleck, S2423); HU (Selleck, S1896); Cisplatin (Supertrack Bio-pharmaceutical, 131102); CX5461 (Selleck, S2684) and H_2O_2 for the times stated for each experiment.

Cell proliferation and viability

Cells treated with siRNA or chemicals were incubated in complete media. Proliferation curves were determined by counting cell number by haemocytometer every 3-5 days upon passage, dependent of the growth rate of individual cell lines. Inhibition rate (%) for each cell line was calculated as (1-siRNA/Control) x 100%. siRNA and Control represent the number of remaining cells for the specific siRNA and siScramble control at the endpoint of the experiment. Relative cell survival: the ratio calculated by dividing the number of cells in the treatment group with untreated control at the endpoint of the experiment.

Flow cytometry

3 x 10^3 cells were plated on 6-well culture plates. After cell adherence, the cells were treated with the indicated condition. Cells were next washed with PBS two times and fixed with 75% ethanol overnight. The cells were washed with PBS three times, and stained with PI (50 ug/ml) for 20 min. Cells were then subjected to flow cytometry (BD FACSCalibur) for cell cycle analysis. Modfit software was used for data processing.

Immunofluorescent staining

Indirect immunofluorescent staining was performed as described elsewhere[46]. Briefly, cells were grown on coverslips and fixed with Carnoy's fluid (methanol:glacial acid:3:1) or 4% paraformaldehyde (PFA) and permeabilize with 0.3% TritonX-100 followed by blocking in PBS with 3% BSA, 3% donkey serum and 0.2% Triton X-100. Primary antibodies were diluted with antibody buffer (0.1% Triton 5% BSA in PBS) and incubated for 2 hours at ambient temperature. Primary antibodies were detected with anti-rabbit-Cy3 or anti-mouse-FITC. Fluorescent images were acquired using an Olympas (BX51) and images were processed analysed using Image-Pro Plus software.

Comet assay

Cells were treated with 10 mM H_2O_2 on ice and subsequently transferred to drug-free complete media for the indicated recovery periods. Cells were then trypsinizied and resuspended in PBS and mixed with an equal volume of 1.6% low-gelling-temperature agarose (Thermo, 16520100) maintained at 42°C. The mixture was immediately spread onto a frosted glass slide (Fisher) pre-coated with 0.8% agarose (Thermo, 16500500) and air dried over-night at RT to set. For alkaline electrophoresis, slides were immersed in pre-chilled lysis buffer (2.5 M NaCl, 10 mM Tris-HCl (pH10), 100 mM EDTA, 1% Triton X-100, 1% DMSO) for 1 h, washed twice with pre-chilled distilled water for 10 min and placed for 20 min in pre-chilled alkaline electrophoresis buffer (300 mM NaOH, 1 mM EDTA). Electrophoresis was then conducted at 0.75 V/cm for 15 min (0.75 V/cm for 30 min for detecting endogenous DNA breaks). Slides were and subsequently neutralized 3 times in 400 mM Tris-HCl pH7.0 for 5 min. For the neutral Comet Assay, electrophoresis solution (300 mM sodium acetate, 100 mM Tris-HCl pH 8.3) was used. DNA was fixed with absolute EtOH for 20min then stained with EtBr(2 ug/ml) for 5 min and washed twice in ddH2O. The percentage of tail moments was calculated by dividing the intensity of tails by that of heads as measured with Image Pro Plus. 100 cells were measured for

each sample. Data presented are the average ±1 s.e.m. of three independent experiments.

Statistics

All histograms are presented as means ± standard deviation. For quantitative analysis including immunoblotting, image analysis and repair analysis at least three independent biological repeats were carried out. Analysis for significant difference between two groups was performed by Two-tailed Student's *t* tests using GraphPad Prism 6 or SPSS 16.0. End-point values of cell survival assays were used for statistical analysis. The level of significance was set as $p<0.05$.

Acknowledgement and Funding

This work is supported by NSF China (31771580, 81702795, 81630038 and 81971433), Department of Science and Technology of Sichuan Province (2019JDTD0020 and 2020YFH0019). A.M.C recognises Wellcome Trust Award 110047/Z/15/Z. We also thank PTM Biolab (Hangzhou) for mass spectrometry analysis.

Author contribution

C.L., A.M.C and Z.T. co-discovered ENDOD1. C.L. and Z.T. established SL between ENDOD1, TP53 and HR defects. M.Z. and X.W. performed biochemical and cell biology assays. C.L. and A.M.C. supervised the overall project and wrote the manuscript.

Competing interests

A patent application 'Application of reagents or drugs inhibiting an endonuclease in cancer therapy (202010295776.6)' was filed on April 15, 2020.

Reference

1. Helleday, T. Putting poly (ADP-ribose) polymerase and other DNA repair inhibitors into clinical practice. *Curr Opin Oncol* **25**, 609-614 (2013).
2. Gelmon, K. A. et al. Olaparib in patients with recurrent high-grade serous or poorly differentiated ovarian carcinoma or triple-negative breast cancer: a phase 2, multicentre, open-label, non-randomised study. *Lancet Oncol* **12**, 852-861 (2011).
3. Shen, Y. et al. BMN 673, a novel and highly potent PARP1/2 inhibitor for the treatment of human cancers with DNA repair deficiency. *Clin Cancer Res* **19**, 5003-5015 (2013).
4. D'Andrea, A. D. Mechanisms of PARP inhibitor sensitivity and resistance. *DNA Repair (Amst)* **71**, 172-176 (2018).
5. Ren, L. et al. The Antiresection Activity of the X Protein Encoded by Hepatitis Virus B. *Hepatology* **69**, 2546-2561 (2019).
6. Fenech, E. J. et al. Interaction mapping of endoplasmic reticulum ubiquitin ligases identifies modulators of innate immune signalling. *Elife* **9**, (2020).
7. Caldecott, K. W. DNA single-strand break repair. *Exp Cell Res* **329**, 2-8 (2014).
8. Bryant, H. E. et al. Specific killing of BRCA2-deficient tumours with inhibitors of poly(ADP-ribose) polymerase. *Nature* **434**, 913-917 (2005).
9. Bouaoun, L. et al. TP53 Variations in Human Cancers: New Lessons from the IARC TP53 Database and Genomics Data. *Hum Mutat* **37**, 865-876 (2016).
10. Sigal, A. & Rotter, V. Oncogenic mutations of the p53 tumor suppressor: the demons of the guardian of the genome. *Cancer Res* **60**, 6788-6793 (2000).
11. Wang, Y. H. et al. Both DNA binding domains of p53 are required for its ultra-rapid recruitment to sites of UV damage. *bioRxiv* 2020.02.09.938993 (2020).
12. Leroy, B. et al. Analysis of TP53 mutation status in human cancer cell lines: a reassessment. *Hum Mutat* **35**, 756-765 (2014).

Figure Legends

Figure 1.

a. Schematic for ENDOD1 protein domains, showing predicted signal peptide (residues 1-22), the endonuclease domain (residues 49-257) and the three C-terminal transmembrane motifs (Ts). Peptides identified by mass spectrometry are shown as red bars. **b**. Indirect immunofluorescence (left) and enumeration (right) for ENDOD1 and PAR foci in untreated RPE1 cells (top row) and RPE1 and *ENDOD1*$^{-/-}$ cells at indicated time after 10 mM H_2O_2 treatment (bottom two rows). For the merged panels nuclear DNA was also counterstained with DAPI. **c**. Left: representative images of alkaline comet assay. Middle: quantification of tail moments for proliferating RPE1 and *ENDOD1*$^{-/-}$ cells at the indicated time points after H_2O_2 challenge. Right: tail moments for low serum-arrested G1 RPE1 and *ENDOD1*$^{-/-}$ cells at indicated time points after H_2O_2 challenge. Percentage of tail moments was calculated by dividing the pixel intensity of tails by that of heads.

Figure 2.

a. Relative survival of G1-arrested *ENDOD1*$^{-/-}$ cells with or without H_2O_2 treatment (10 μM). Cells were transfected with the indicated siRNAs 48 hours before challenge. **b**. Relative survival of RPE1 cells subjected to the indicated siRNA treatments. siRNA were transfected three times with three day intervals. **c**. Quantification of 53BP1 and γH2AX foci in *ENDOD1*$^{-/-}$ cells 72 hours following either control or si*BRCA1* treatment. **d**. Representative images of 53BP1 foci following transfection of *ENDOD1*$^{-/-}$ cells with si*BRCA1* or si*BRCA2*.

Figure 3.

a. Correlation of *TP53*/HR mutations with cytotoxicity of si*ENDOD1* in terms of inhibition rate (%) for tested normal and cancer cell lines. **b**. Relative survival of the indicated proliferating cells 7 days after two rounds of si*TP53* transfection (separated by 3 days). **c**. Equivalent experiment as in b, using cells arrested in G1 by serum starvation. **d**. Representative images of alkaline (left) or neutral (right) comet assays for the indicated G1 arrested cells with or without prior si*TP53* transfection. **e**. Quantification for the percentage of tail moments calculated by dividing the pixel intensity of tails by that of heads.

Figure 4.

a. Representative images of immunofluorescent staining for pRPA32 in the indicated

G1 arrested cell lines 96 hours following siRNA transfection. **b**. Quantification of pRPA32 foci from the experiment shown in a. **c**. Quantifications of pRPA32 and 53BP1 foci in the indicated G1 arrested cell lines 0, 48, 72 and 96 hours after si*TP53* or control transfection. **d**. Representative images for pRPA32 in si*ENDOD1* treated cancer cell lines that harbour *TP53* mutations. A549 is a *TP53* wildtype control.

Supplementary Figure legends

Supplementary Figure 1.

ENDOD1 peptides sequences captured by TMT mass spectrometry in T43 cells following 6 days treatment with Olaparib.

Supplementary Figure 2.

a. Survival based on counting RPE1 or *ENDOD1*$^{-/-}$ cells subjected to the indicated genotoxic treatments. **b**. Survival of serum starved (left) or proliferating (middle) RPE1 and si*ENDOD1* or si*Scramble* transfected GES-1 cells (right) treated with the indicated concentrations of H_2O_2 for 72 hours.

Supplementary Figure 3.

a. RPE1 cells were passaged and transfected with indicated siRNA at 3 days intervals. Cells were stained with crystal blue at day 12. **b.** Proliferation quantified by haemocytometer cell counting over 3 weeks for the indicated immortalised non-cancerous cells with or without *ENDOD1* silencing. Control experiments using RPE1 and *ENDOD1*$^{-/-}$ are shown in the first two panels. **c**. FACS analysis for RPE1 and *ENDOD1*$^{-/-}$ cell cycle. Distribution of cells in G1, S and G2 phases are shown.

Supplementary Figure 4.

a. Proliferation curves for the indicated cancer lines following either si*ENDOD1* or control transfection. Cells were passaged, counted by haemocytometer and transfected at 3 day intervals. The reported status of the *TP53* gene is indicated for each cell line [12] (also see: https://www.lgcstandards-atcc.org). Cell numbers for NCI-H1299, HL60 and MDA-MB-231 were counted 10 days after transfection. **b**. Equivalent experiments on cancer cells with functional HR and p53. **c.** FACS analysis for RPE1 and *ENDOD1*$^{-/-}$ cells following the indicated siRNA treatment. **d**. Crystal blue staining of Indicated cell lines following siRNA against the indicated genes. Cell were transfected at 3 day intervals and stained on day 10.

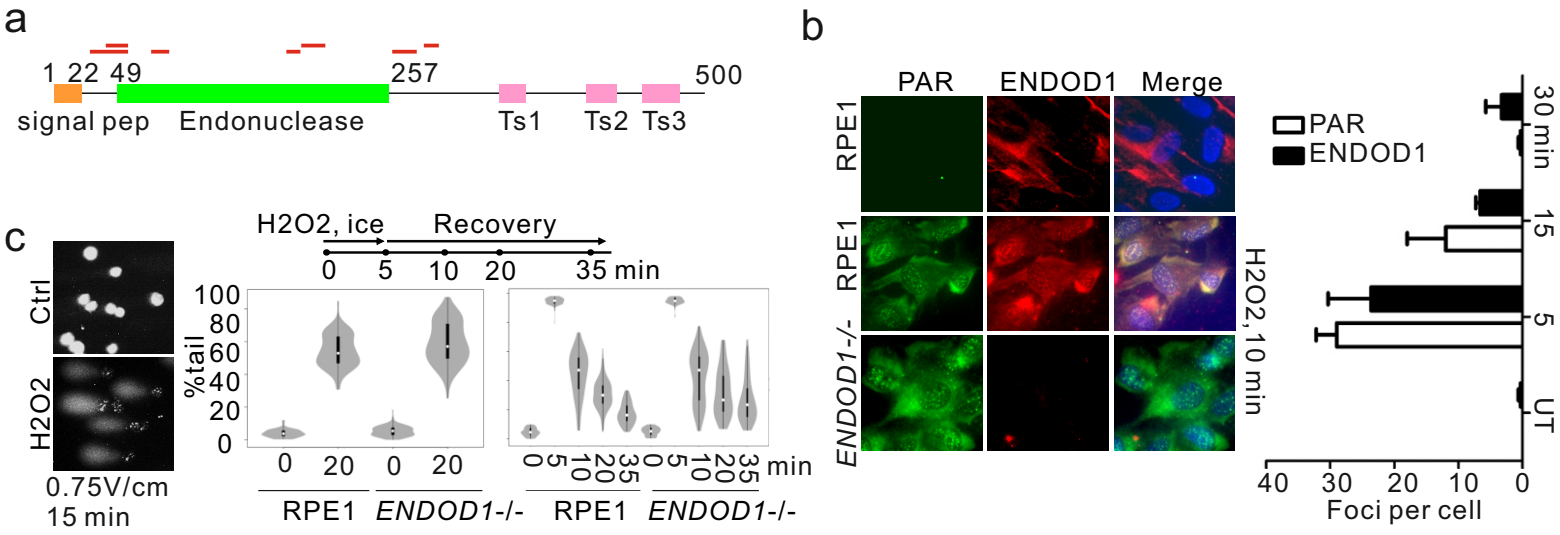
a
1 22 49
257
500
signal pep
Endonuclease
Ts1
Ts2
Ts3
b
PAR
ENDOD1
Merge
RPE1
RPE1
ENDOD1-/-
PAR
ENDOD1
H2O2, 10 min
30 min
15
5
UT
40
30
20
10
0
Foci per cell
c
Ctrl
H2O2
0.75V/cm
15 min
H2O2, ice
Recovery
0
5
10
20
35 min
%tail
100
80
60
40
20
0
0
20
0
20
RPE1
ENDOD1-/-
RPE1
ENDOD1-/-
0
5
10
20
35
0
5
10
20
35
min

Figure 1

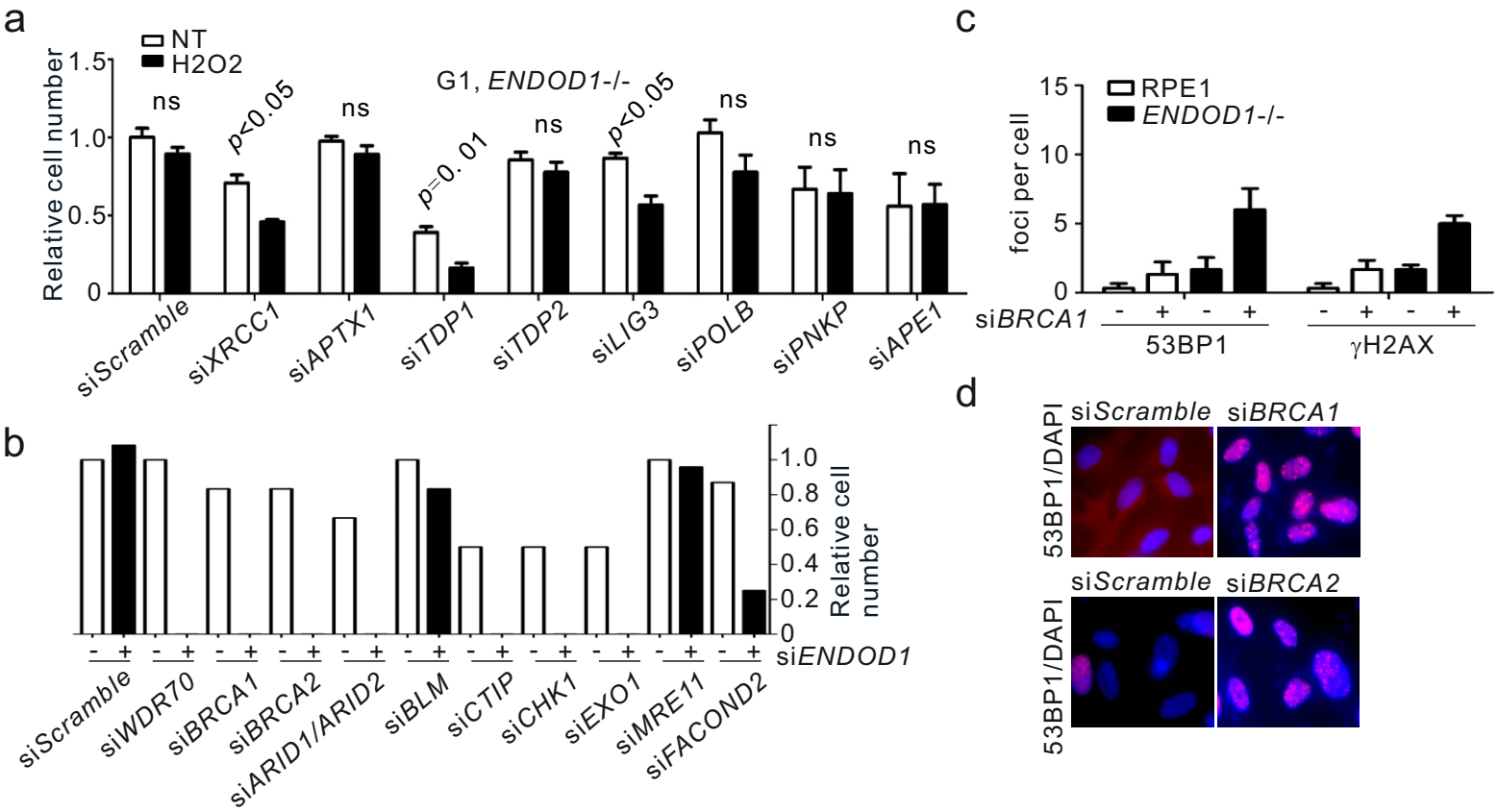
a
NT
H2O2
Relative cell number
1.5
1.0
0.5
0
G1, ENDOD1-/-
ns
p<0.05
ns
p=0. 01
ns
p<0.05
ns
ns
ns
siScramble
siXRCC1
siAPTX1
siTDP1
siTDP2
siLIG3
siPOLB
siPNKP
siAPE1
b
1.0
0.8
0.6
0.4
0.2
0
Relative cell number
siENDOD1
siScramble
siWDR70
siBRCA1
siBRCA2
siARID1/ARID2
siBLM
siCTIP
siCHK1
siEXO1
siMRE11
siFACOND2
c
RPE1
ENDOD1-/-
foci per cell
15
10
5
0
siBRCA1
53BP1
γH2AX
d
siScramble
siBRCA1
53BP1/DAPI
siScramble
siBRCA2
53BP1/DAPI

Figure 2

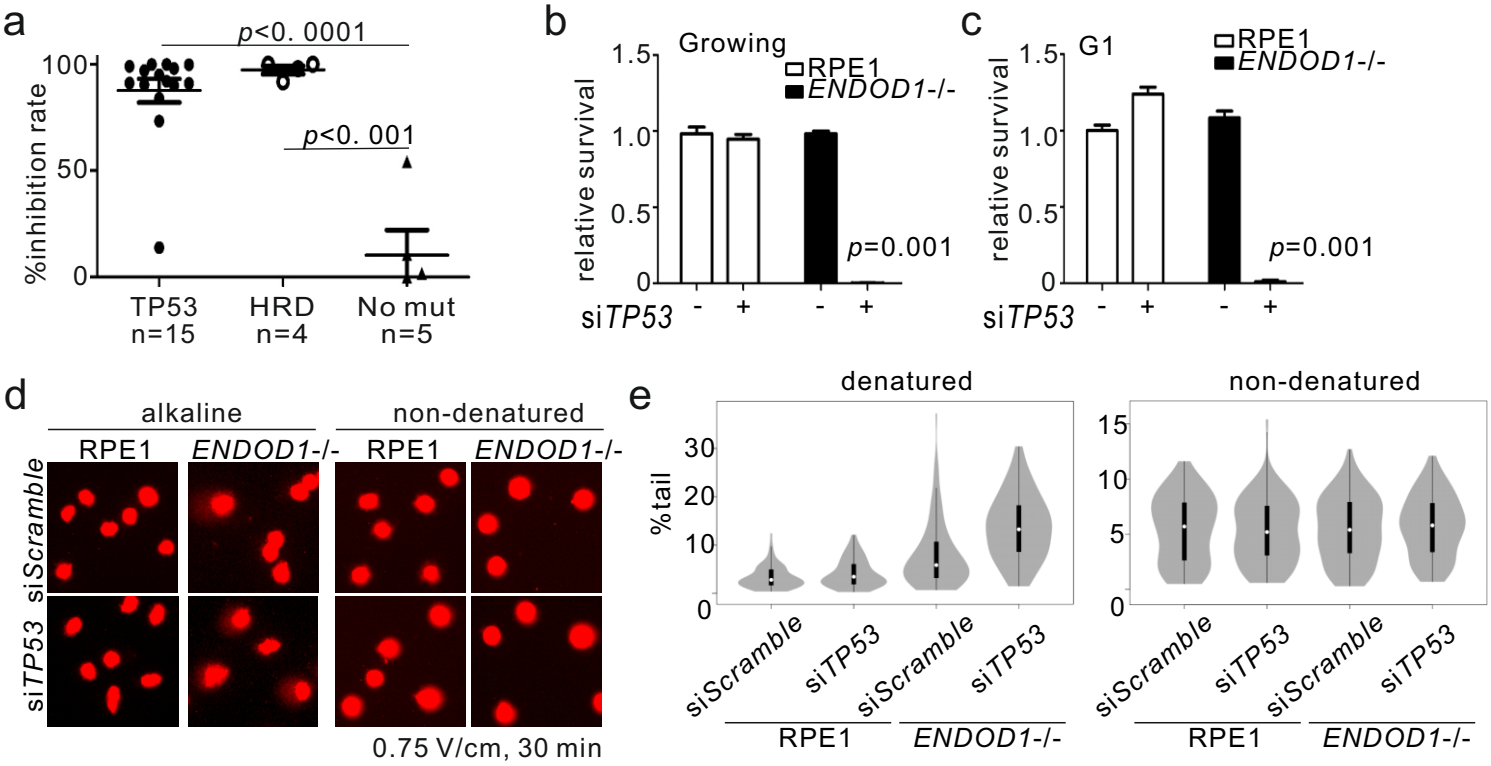
a
p<0. 0001
p<0. 001
%inhibition rate
100
50
0
TP53
n=15
HRD
n=4
No mut
n=5
b
Growing
RPE1
ENDOD1-/-
relative survival
1.5
1.0
0.5
0
p=0.001
siTP53
-
+
-
+
c
G1
RPE1
ENDOD1-/-
relative survival
1.5
1.0
0.5
0
p=0.001
siTP53
-
+
-
+
d
alkaline
non-denatured
RPE1
ENDOD1-/-
RPE1
ENDOD1-/-
siScramble
siTP53
0.75 V/cm, 30 min
e
denatured
non-denatured
%tail
30
20
10
0
15
10
5
0
siScramble
siTP53
siScramble
siTP53
RPE1
ENDOD1-/-
siScramble
siTP53
siScramble
siTP53
RPE1
ENDOD1-/-

Figure 3

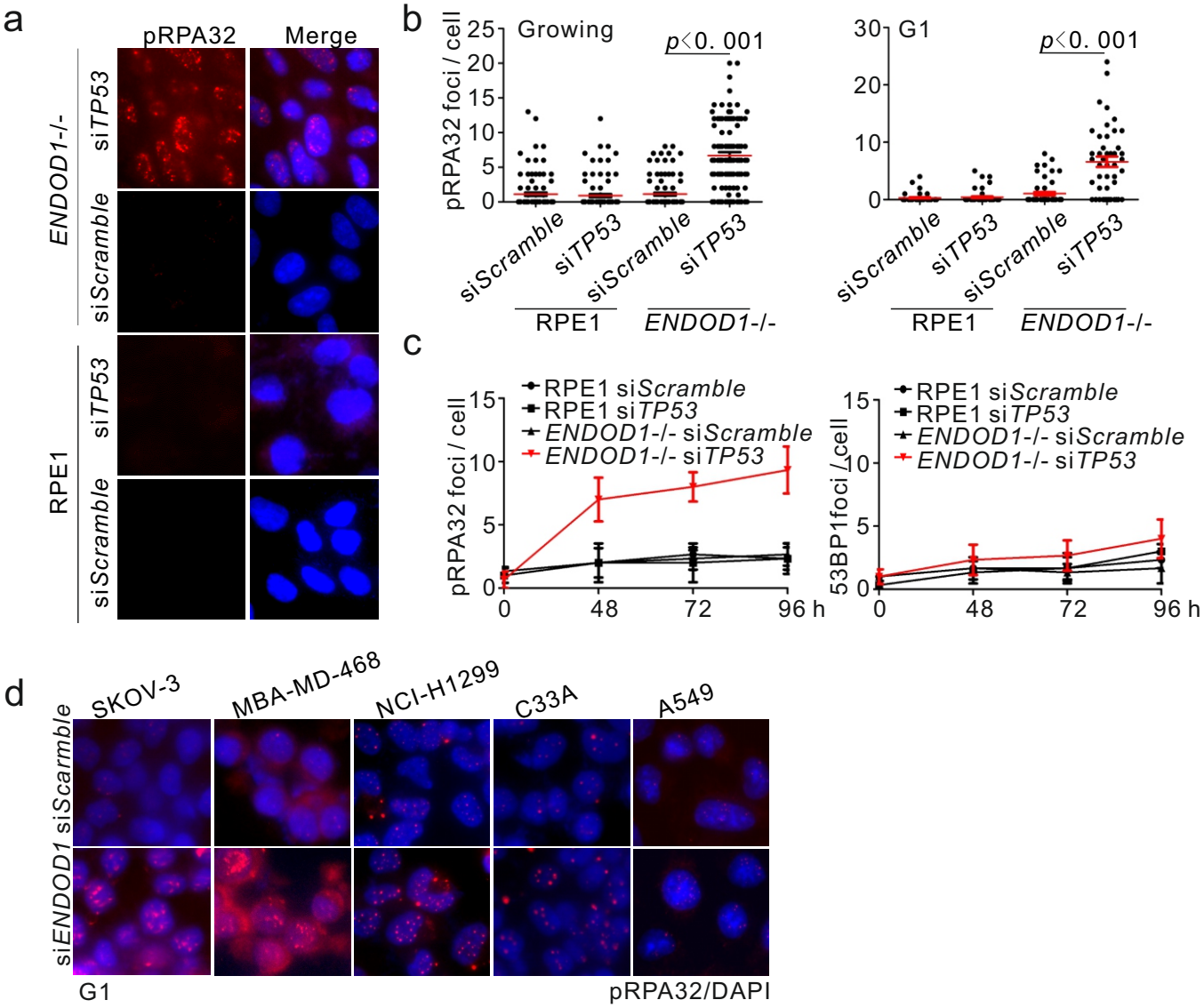
a
pRPA32
Merge
ENDOD1-/-
siTP53
siScramble
RPE1
siTP53
siScramble
b
Growing
p<0. 001
pRPA32 foci / cell
siScramble
siTP53
siScramble
siTP53
RPE1
ENDOD1-/-
G1
p<0. 001
siScramble
siTP53
siScramble
siTP53
RPE1
ENDOD1-/-
c
RPE1 siScramble
RPE1 siTP53
ENDOD1-/- siScramble
ENDOD1-/- siTP53
pRPA32 foci / cell
0
48
72
96 h
RPE1 siScramble
RPE1 siTP53
ENDOD1-/- siScramble
ENDOD1-/- siTP53
53BP1foci /cell
0
48
72
96 h
d
SKOV-3
MBA-MD-468
NCI-H1299
C33A
A549
siScarmble
siENDOD1
G1
pRPA32/DAPI

Figure 4

23 LVGEEEAGFGECDKFFYAGTPPAG LAADSHVK 54

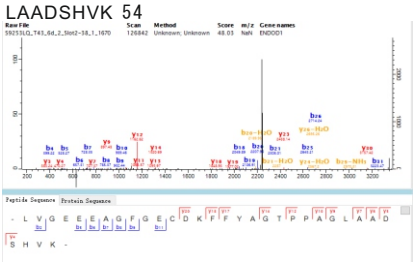

174 WYVNLHSLMDR 184

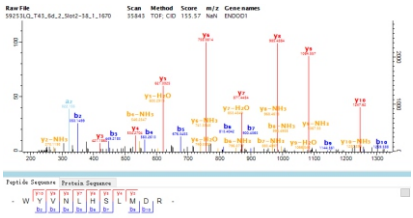

185 ALTPQCGSGFDLYILTGTVPSDYR 208

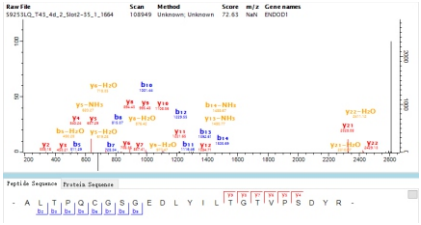

73 DRIPVYSAFR 82

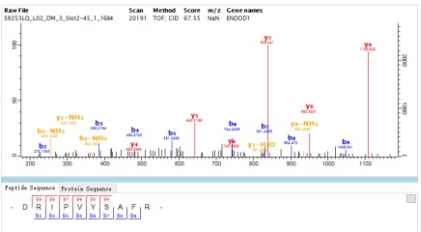

37 FFYAGTPPAGLAADSHVK 54

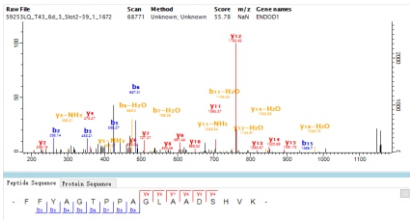

281 ILEVVNQIQDEER 294

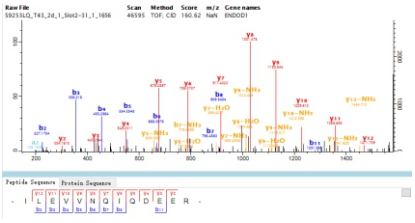

257 LLPFNPQLFQNNCGETEQDTEK 278

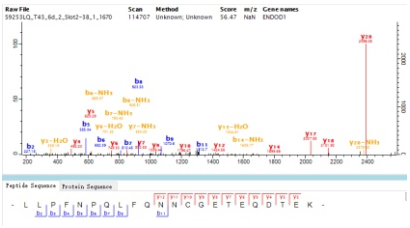

Figure S1

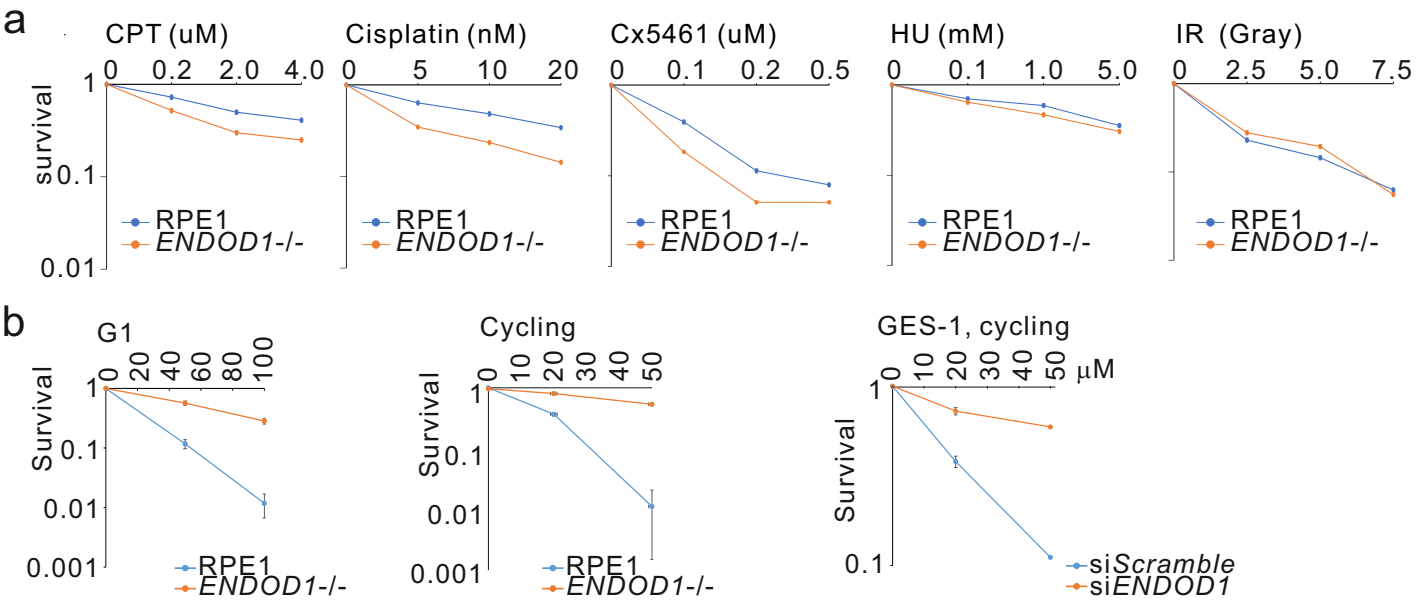
a
CPT (uM)
0 0.2 2.0 4.0
Cisplatin (nM)
0 5 10 20
Cx5461 (uM)
0 0.1 0.2 0.5
HU (mM)
0 0.1 1.0 5.0
IR (Gray)
0 2.5 5.0 7.5
survival
1
0.1
0.01
RPE1
ENDOD1-/-
b
G1
0 20 40 60 80 100
Cycling
0 10 20 30 40 50
GES-1, cycling
0 10 20 30 40 50 μM
Survival
1
0.1
0.01
0.001
RPE1
ENDOD1-/-
siScramble
siENDOD1

Figure S2

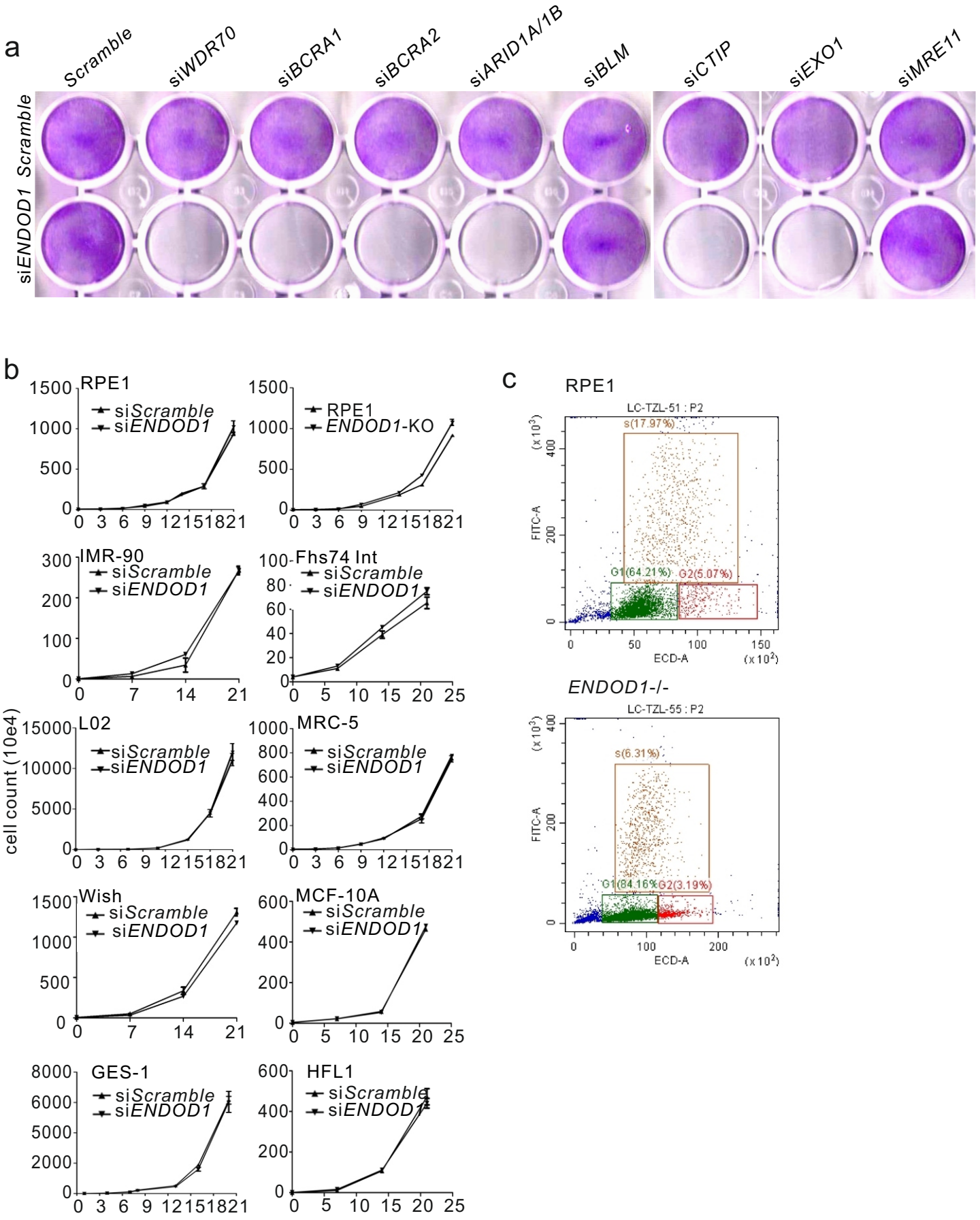
a
Scramble
siWDR70
siBCRA1
siBCRA2
siARID1A/1B
siBLM
siCTIP
siEXO1
siMRE11
Scramble
siENDOD1
b
RPE1
siScramble
siENDOD1
RPE1
ENDOD1-KO
IMR-90
Fhs74 Int
L02
MRC-5
Wish
MCF-10A
GES-1
HFL1
cell count (10e4)
c
RPE1
LC-TZL-51 : P2
s(17.97%)
G1(64.21%)
G2(5.07%)
FITC-A
ECD-A
ENDOD1-/-
LC-TZL-55 : P2
s(6.31%)
G1(84.16%)
G2(3.19%)

Figure S3

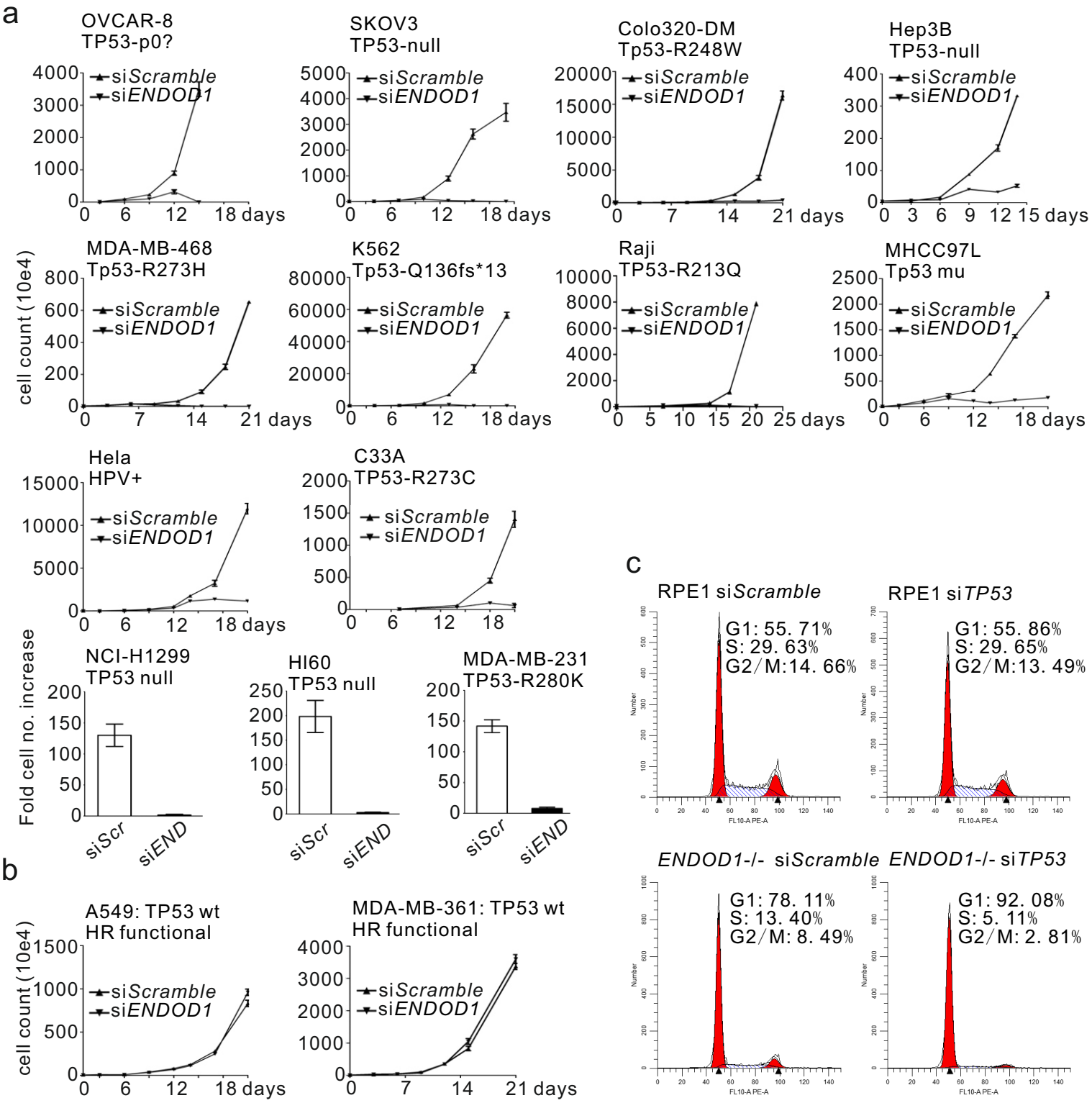
a
OVCAR-8
TP53-p0?
SKOV3
TP53-null
Colo320-DM
Tp53-R248W
Hep3B
TP53-null
MDA-MB-468
Tp53-R273H
K562
Tp53-Q136fs*13
Raji
TP53-R213Q
MHCC97L
Tp53 mu
Hela
HPV+
C33A
TP53-R273C
siScramble
siENDOD1
cell count (10e4)
days
NCI-H1299
TP53 null
HI60
TP53 null
MDA-MB-231
TP53-R280K
Fold cell no. increase
siScr
siEND
b
A549: TP53 wt
HR functional
MDA-MB-361: TP53 wt
HR functional
c
RPE1 siScramble
G1: 55. 71%
S: 29. 63%
G2/M:14. 66%
RPE1 siTP53
G1: 55. 86%
S: 29. 65%
G2/M:13. 49%
ENDOD1-/- siScramble
G1: 78. 11%
S: 13. 40%
G2/M: 8. 49%
ENDOD1-/- siTP53
G1: 92. 08%
S: 5. 11%
G2/M: 2. 81%
d
RPE1
siTP53
siENDOD1
ENDOD1-/-

Figure S4